PCCP

The electro-oxidation of formic acid on Pt–Pd single crystal bimetallic surfaces

M. Arenz,*[a] V. Stamenkovic,[a] T. J. Schmidt,†[a] K. Wandelt,[b] P. N. Ross[a] and N. M. Markovic[a]

[a] *Materials Science Division, Lawrence Berkeley National Laboratory, University of California, Berkeley, CA 94720, USA. E-mail: marenz@lbl.gov*
[b] *Institut für Physikalische und Theoretische Chemie, Universität Bonn, Wegelerstr.12, D-53115, Bonn, Germany*

Received 4th June 2003, Accepted 12th August 2003
First published as an Advance Article on the web 28th August 2003

The interrelationship between the macroscopic kinetic rate of HCOOH oxidation in 0.1 M $HClO_4$ solution and the morphology/composition of the electrode is studied on Pt(111) modified by Pd (denoted hereafter as the Pt(111)–$Pd_{x\mathrm{ML}}$ system, $0 < x < 1$) and on Pt–Pd bulk single crystal alloy surfaces (denoted hereafter as the $PtPd_{x\mathrm{at\%}}$(111) system, $x = 6$ and $x = 25$). The Pd surface composition of the Pt(111)–$Pd_{x\mathrm{ML}}$ and $PtPd_{x\mathrm{at\%}}$(111) electrodes was established previously *ex-situ* by low energy ion scattering (LEIS) measurements. The nature of adsorbed intermediates (CO_{ad}) and the electrocatalytic properties (the onset of CO_2 formation) at the Pt(111)–$Pd_{x\mathrm{ML}}$ and the $PtPd_{x\mathrm{at\%}}$(111) interface were studied by FTIR spectroscopy. The results show that Pd atoms either *on* the surface or *in* the surface have an unique catalytic activity for HCOOH oxidation, with Pd atoms being three (bulk alloys) or five times (Pd films) more active than Pt atoms at 0.4 V. FTIR spectra reveal that on Pt atoms adsorbed CO is produced from dehydration of HCOOH, whereas *no* CO adsorbed on Pd can be detected although a high production rate of CO_2 is observed at low potentials, indicating that the reaction can proceed on Pd at low potentials without the Pt typical ''poison'' formation.

1. Introduction

The electro-oxidation of small organic molecules such as carbon monoxide, formaldehyde, formic acid and methanol have been extensively studied in the past (for an overview see ref. 1–3) and are still of high importance[4–6] as model systems for understanding the relationship between the surface structure/composition of metal catalysts and the kinetic reaction rate. It is now well established that on platinum the electro-oxidation of HCOOH to CO_2 proceeds *via* the so-called *dual-path mechanism* proposed originally by Capon and Parsons.[7] In this reaction scheme the ''direct'' path is a fast reaction involving one or more ''active intermediates'', while the second reaction pathway involves the formation of CO_{ad} which, depending on the electrode potential, may act either as a site blocking species or as an active intermediate.[1,3] The self-poisoning behavior on Pt is well documented by FTIR studies using low-index and stepped single crystal surfaces.[8–12] These studies showed that the introduction of monoatomic steps in the structure of low-index single crystal surfaces leads to a decrease in the activity due to an increase in the CO formation at the step sites. As a consequence, introducing ''defect sites'' in order to increase the catalytic activity of Pt low index single crystal surfaces is not feasible. Another, generally more successful method to enhance the catalytic activity of Pt is to create bimetallic surfaces that will (ideally) optimize the adsorption of HCOOH while oxidizing CO_{ad} with a minimum surface coverage by OH_{ad}, *e.g.*, the nearly autocatalytic oxidation of CO_{ad}.[4,13–18] The influence of these surface modifiers can generally be ascribed to one or more of the following reasons: (*i*) electronic (ligand) effects where the second component alters the electronic properties of the catalytically active metal, (*ii*) bifunctional effects where each of the surface species provides one of the necessary reactant sites, and (*iii*) ensemble (site-size) effects where a minimum number of atoms of one species is required for the reaction to proceed.

In this study the electronic, ensemble and bifunctional effects in formic acid oxidation will be tested on both pseudomorphic Pd films supported on Pt(111) as well as on (111) oriented Pt–Pd bulk single crystal alloy surfaces. The catalytic properties of both systems are examined by potentiodynamic and potentiostatic measurements. The results unambiguously show that Pd atoms either *on* the surface (the Pt(111)–$Pd_{x\mathrm{ML}}$ systems) or *in* the surface (the $PtPd_{x\mathrm{at\%}}$(111) systems) of the Pt(111) crystal have an unique catalytic activity for formic acid oxidation. The identity of adsorbed intermediates and the potential for the onset of CO_2 formation were obtained by FTIR spectroscopy.

2. Experimental

2.1 Electrochemical measurements

In the presented work ultrathin Pd films deposited on Pt(111) as well as $PtPd_{x\mathrm{at\%}}$(111) alloy ''beads'' were used as working electrodes. The Pd concentration in the bulk of the alloys was 6% and 25% as determined by LEIS spectra of the sputter-cleaned surface. The alloy samples and the Pt(111) crystal were prepared by flame annealing in a hydrogen flame and subsequent cooling in a mild stream of a mixture of Ar and H_2. Since the surface composition of alloys usually deviates from the bulk composition due to segregation effects,[19] the surface composition of the samples has been also determined after flame annealing and transfer to ultra high vacuum (UHV) by LEIS leading to values of $x \sim 15\%$ and $x \sim 44\%$ for the

† Present address: Celanese Ventures GmbH, Frankfurt, Germany.

 DOI: 10.1039/b306307k

This journal is © The Owner Societies 2003

6% and 25% bulk alloy, respectively (for more details see ref. 20). For the electrochemical measurements after flame annealing the electrodes were transferred into the electrochemical cell protected by a drop of ultrapure water. The preparation of the Pt(111)–$Pd_{x ML}$ surfaces has been described before.[21,22] In short, the Pt(111) crystal was cycled in a 0.05 M $H_2SO_4 + 5 \times 10^{-6}$ M PdO solution at a scan rate of 50 mV s^{-1}. The amount of Pd deposited was controlled by the continuous change of the voltammetric features, from those characteristic of Pt(111) to those characteristic for a pseudomorphic monolayer of palladium. The palladium coverage, indicated in the text, is calculated using a calibration curve which compares the Pd coverage of UHV prepared films with the current response in cyclic voltammetry recorded on the same surface after a transfer into an electrochemical cell (for details see ref. 21).

The oxidation of formic acid was conducted in a thermostated standard three-compartment electrochemical cell. A circulating constant temperature bath (Fisher Isotemp Circulator) maintained the temperature of the electrolyte within $\pm 0.5\,^{\circ}C$. All measurements were conducted nonisothermally, *i.e.*, keeping the temperature of the reference electrode constant (≈298 K) while that of the working electrode was varied from 276 K to 303 K. The reference electrode was a saturated calomel electrode (SCE) separated by a closed bridge to prevent chloride contamination of the electrolyte. All potentials shown in the text, however, refer to the reversible hydrogen electrode in the same solution, calibrated from measuring the reversible potential for the hydrogen evolution/oxidation reaction in a rotating disk electrode configuration. The experimental procedure for formic acid oxidation was as follows. After preparation the electrode was immersed under potential control at 20 mV into Ar-purged (Air Products 5N5 purity) 0.1 M $HClO_4$ containing 50 mM HCOOH. Prior to recording the polarization curves the electrode was polarized for 30 s at a potential of 900 mV in order to oxidize (pre)adsorbed CO and to produce comparable results. The aqueous solutions were prepared from $HClO_4$ (Aldrich, double destilled), HCOOH (Aldrich, ACS grade), H_2SO_4 (Baker Ultrex), PdO (Alfa Products), using pyrolitically triply destilled water.

2.2 FTIR measurements

For the *in-situ* FTIR measurements, we used a Nicolet Nexus 670 spectrometer equipped with a LN_2-cooled MCT detector. All IR measurements were performed in a spectroelectrochemical glass cell designed for an external reflection mode in a thin layer configuration. The cell is coupled at its bottom with a CaF_2 prism beveled at 60° from the surface normal. The experimental procedure for the IR measurements was adapted from the measurements of the polarization curves. Prior to each experiment the solution was saturated with argon in order to deoxygenate the solution. The electrodes were immersed into the electrolyte and pressed onto the prism under potential control at a potential of 0.00 V and the electrode potential was increased in steps of about 100 mV.

The spectra were recorded with a resolution of 8 cm^{-1}. All measurements were performed using p-polarized light. In order to obtain a single beam spectrum 100 scans were collected at each potential resulting in a recording time of *ca.* 1 min. Absorbance spectra were calculated as the ratio $-\log(R/R_0)$ where R and R_0 are the reflectance values corresponding to the sample and reference spectra, respectively. The reference spectra were recorded either at a potential of 1.0 V, where CO_{ad} is completely oxidized, or at 0.00 V, a potential where no CO_2 production occurs. The reference potential in the spectroelectrochemical cell was controlled by a reversible hydrogen electrode (RHE).

3. Results

3.1 Voltammetric studies

To illustrate how the nature of Pd surface atoms influences the electrochemical properties of Pt(111), the cyclic voltammograms of both $PtPd_{6at\%}(111)$ and $PtPd_{25at\%}(111)$ bulk alloys as well as Pt(111)–$Pd_{\sim 0.15\ ML}$ and Pt(111)–$Pd_{\sim 1\ ML}$ electrodes are compared to the voltammogram of the Pd unmodified Pt(111) surface in perchloric acid solution (dashed line Fig. 1). While this comparison is detailed elsewhere,[22] the following brief description forms a necessary precursor to the interpretation of related kinetic measurements, considered in the next section. As discussed in previous work,[22] there are three characteristics of Pd surface atoms discernible in the cyclic voltammetry. First, Fig. 1 shows that with increasing surface coverage by Pd (Θ_{Pd}) either *on* the surface (Fig. 1a and 1b) or *in* the surface (Fig. 1c and 1d) the charge in the hydrogen underpotential region (H_{upd}) increases from about 0.66 ML for Pt(111) (*i.e.*, 0.66 H_{upd} per Pt) to about 1 ML H_{upd} for a complete Pd film on Pt(111)[22] (1 H_{upd} per Pd). We assigned this finding previously to a stronger Pd–H_{upd} interaction compared to the Pt–H_{upd} interaction.[21,22] Secondly, while the peak potential of the "butterfly" feature ($E \sim 0.5$–0.8 V) shifts to more negative potentials with increasing palladium surface coverage, the charge under the peak decreases from *ca.* 80 μC cm^{-2} on Pt(111) to *ca.* 60 μC cm^{-2} on pseudomorphic Pd monolayer.

Since there has been some controversy about the interpretation of the underlying processes shaping the "butterfly" peak in the voltammogram of Pt(111), the interpretation of the pseudocapacitance in the 'butterfly" potential region is not straightforward. Nevertheless, closely following our recent discussion[22] we propose that the observed behavior can be explained by an increased adsorption strength of anions on Pd relative to Pt atoms. In particular, due to the higher oxophilicity of Pd the adsorption of oxygenated species (hereafter denoted as OH_{ad}) is shifted to lower potentials (as clearly observed in alkaline solution[21]). However, because in perchloric acid solution OH^- adsorption is in strong competition with the adsorption of perchlorate[23] and chloride anions (the latter

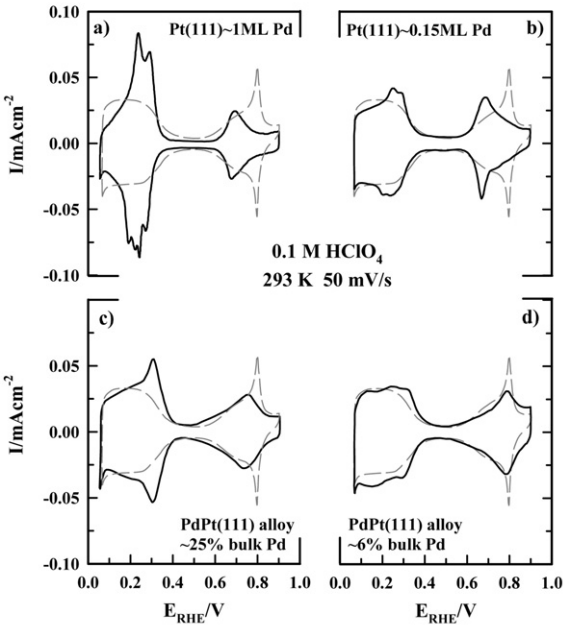

Fig. 1 Cyclic voltammogram of bare Pt(111) (dashed line) in 0.1 M $HClO_4$ compared to $PtPd_{xat\%}(111)$ bulk alloys and thin palladium films deposited at Pt(111). Sweep rate 50 mV s^{-1} at room temperature. (a) Pt(111)–$Pd_{\sim 1\ ML}$, (b) Pt(111)–$Pd_{\sim 0.15\ M}$, (c) $PtPd_{25at\%}(111)$ and (d) $PtPd_{6at\%}(111)$.

present as an impurity in $HClO_4$[22]), coverage by OH_{ad} on Pd is suppressed with co-adsorbed ClO_4^- and Cl^-. For further details see ref. 22.

3.2 Formic acid oxidation

3.2.1. Polarization curves. For the purpose of demonstrating the effects of Pd atoms on the catalytic properties of Pt(111) two sets of polarization curves are summarized in Fig. 2. In agreement with previous reports,[24–26] for relatively fast sweep rates (10 mV s^{-1}) the oxidation of HCOOH on Pt(111) modified with Pd films is significantly activated. For example, Fig. 2a shows that the onset of HCOOH oxidation on the Pt(111)–$Pd_{\sim 1\ ML}$ surface starts at *ca.* 0.2 V, producing a relatively sharp peak at 0.3 V (note that the current density is divided by 3!). Interestingly, the palladium film is extremely active for formic acid oxidation only at low potentials, *i.e.* once the maximum activity is reached the deactivation is very fast and above 0.5 V the catalytic activity is essentially zero. On the Pt(111)–$Pd_{\sim 0.2\ ML}$ surface (Fig. 2b), however, the polarization curve can be divided into two potential regions: (i) $0.2 < E < 0.4$ V where HCOOH oxidation quickly reaches a maximum at about 0.3 V and then activity steeply decreases, and (ii) $0.4 < E < 0.9$ V where the activity increases again with a second maximum appearing at about 0.55 V. Clearly, while the catalytic activity in the first potential region is Pd-like, the catalytic activity above 0.4 V is very similar with one observed for Pt(111) under the same experimental conditions.[27] Notice that the catalytic properties of a Pt(111) electrode modified with 0.2 ML of Pd gradually change from those characteristic of bare Pt(111) to those which are characteristic for Pt(111) covered with 1 ML of Pd, indicating that Pd atoms cluster into islands during deposition and that Pt and Pd behave according to their singular surface chemistry. Further inspection of Fig. 2a and 2b reveals that at a low scan rate of 1 mV s^{-1} (quasi steady-state condition) the shape of polarization curves is more or less the same as at a scan rate of 10 mV s^{-1}. The catalytic activity is, however, considerably reduced at very slow sweep rates, indicating that in the course of the oxidation of formic acid poisoning of the surface takes place. This deactivation may be related either to the formation of "poisoning" reaction intermediates (*e.g.*, CO_{ad}) or to the adsorption of spectator species such as OH_{ad}, $ClO_{4,\ ad}$ and Cl_{ad}.

Fig. 2c and 2d show that the oxidation of HCOOH on $PtPd_{6at\%}$(111) and $PtPd_{25at\%}$(111) bulk alloys at a relatively fast scan rate (10 mV s^{-1}) occurs *via* a single rather broad peak with a catalytic activity that is neither Pd nor Pt-like, *i.e.*, PtPd(111) bulk alloys behave as a pseudometal. Fig. 2d shows that on $PtPd_{6at\%}$(111) the oxidation of HCOOH, which starts at *ca.* 0.35 V, increases monotonically up to 0.6 V and then starts to decrease again. At a slow sweep rate (1 mV s^{-1}) the reaction is inhibited at low potentials and the maximum in the current density shifts slightly to higher potentials. The form of the polarization curve, however, remains more or less the same. Increasing the Pd bulk composition up to 25at% (Fig. 2c) leads to a significant increase in the activity, with the onset of HCOOH oxidation being close to 0.2 V and with the maximum catalytic activity at *ca.* 0.4 V. The shape and the apparent activity of $PtPd_{25at\%}$(111) is, however, dependent on the sweep rate v and for $v = 1$ mV s^{-1} formic acid oxidation is strongly inhibited at low potentials with the maximum activity observed at 0.7 V. As mentioned above, the deactivation at slow sweep rates may be caused by the blocking of active sites either by the formation of "poisoning" reaction intermediates (*e.g.*, CO) or by the adsorption of spectator species (*e.g.*, OH_{ad}, $ClO_{4,\ ad}$ and Cl_{ad}).

In order to examine the inhibiting effects of CO_{ad} and OH_{ad} on the electro-oxidation of HCOOH, it is instructive to compare the catalytic activity under different potential sweep directions, as shown in Fig. 3 for the $PtPd_{6at\%}$(111) and Pt(111)–$Pd_{\sim 1\ ML}$ surfaces. For the former surface (Fig. 3a) the catalytic activity is higher in the negative sweep direction than in the positive sweep direction. This difference in catalytic activity can be explained by taking into account the surface state of the catalysts in the different sweep directions. That is, while in the anodic scan the activity is predominately controlled by a high surface coverage of CO_{ad}, in the cathodic scan direction the activity is predominantly controlled by a high surface coverage of OH_{ad}. The comparison of Fig. 1d and 3a reveals that during the negative sweep direction the onset of the oxidation

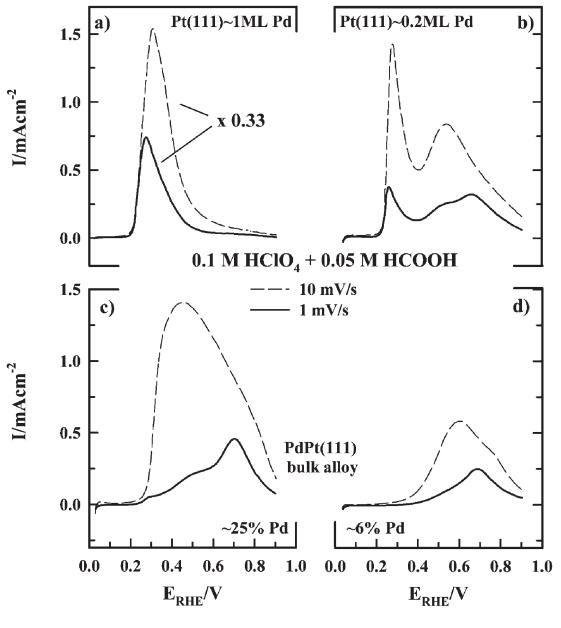

Fig. 2 Polarization curves recorded at 293 K in 0.1 M $HClO_4$ containing 50 mM HCOOH. Sweep rates 10 mV s^{-1} (dashed line) and 1 mV s^{-1} (solid line). (a) Pt(111)–$Pd_{\sim 1\ ML}$, (b) Pt(111)–$Pd_{\sim 0.2\ ML}$, (c) $PtPd_{25at\%}$(111) and (d) $PtPd_{6at\%}$(111) Pd.

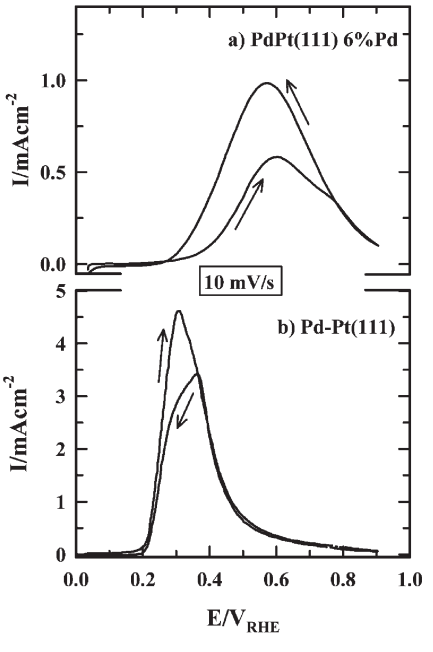

Fig. 3 Polarization curves at anodic and cathodic potential sweep in 0.1 M $HClO_4$ containing 50 mM HCOOH. Sweep rate 10 mV s^{-1} at 293 K. (a) $PtPd_{6at\%}$(111) Pd. (b) Pt(111)–$Pd_{\sim 1\ ML}$.

of HCOOH coincides with the onset of OH_{ad} reduction and the regeneration of bare metal sites. A similar behavior is also observed on Pt(111).[27] In contrast to the behavior on the bulk alloy, on the Pt(111)–$Pd_{\sim 1\ ML}$ surface the activity is high in a wide potential range independent on the sweep direction. Only between $0.25 < E < 0.4$ V the positive scan is more active than the negative scan. As will be discussed in section 4, these findings may indicate that the activity of the Pt(111)–$Pd_{\sim 1\ ML}$ surface in both directions is controlled by the surface coverage of spectator OH_{ad}, $ClO_{4,\ ad}$ and Cl_{ad} species rather than by CO_{ad}. In what follows, direct information regarding the "self-poisoning" effects will be established by utilizing FTIR spectroscopy. On the other hand, the relationship between OH_{ad} surface coverage and the rate of HCOOH oxidation will be revealed by the effect of temperature.

3.2.2. FTIR measurements. Potential dependent series of FTIR spectra on unmodified Pt(111), Pt(111)–$Pd_{\sim 0.5\ ML}$ and Pt(111)–$Pd_{\sim 1\ ML}$, respectively, in $HClO_4$ solution containing 50 mM HCOOH are shown in Fig. 4a–4f. For each surface at the left hand side of the series spectra are referenced to a single beam spectrum recorded at 0.00 V, whereas at the right hand side the spectra are referenced to a single beam spectrum recorded at 1.00 V. The intensities of the spectra in HCOOH containing solution are adjusted to each other (the left handed spectra are divided by the factor of 20) in order to display the potential dependent occurrence of the CO_2 as well as the CO band in the same series. At the bottom (Fig. 4b, d, f) spectra of a saturated CO adlayer adsorbed on the respective surfaces from CO saturated perchloric acid solution are shown as a reference (intensities divided by a factor of 2). Note, since only the terminal feature of CO on Pt is of central concern here, and the spectral region for bridging/three-fold-hollow CO on Pt does not shed light on the differences between Pt and Pt–Pd bimetallic surfaces, the latter is not shown in order to enhance clarity. From the spectra of the CO adlayer formed in solution containing CO it can be seen that the absorption frequency for the C–O stretching vibration on Pt is located at about 2070 cm^{-1}, whereas the C–O stretching vibration on Pd is located at about 1920 cm^{-1}, and therefore both bands are easy to distinguish (for further details see ref. 22,28). CO_2 in solution can be detected due to an absorption band at about 2343 cm^{-1}.

Fig. 4a shows that on Pt(111) adsorbed CO is produced from dehydration of HCOOH, as evidenced by C–O stretch features at 2050–2063 cm^{-1}. Notice that formic acid

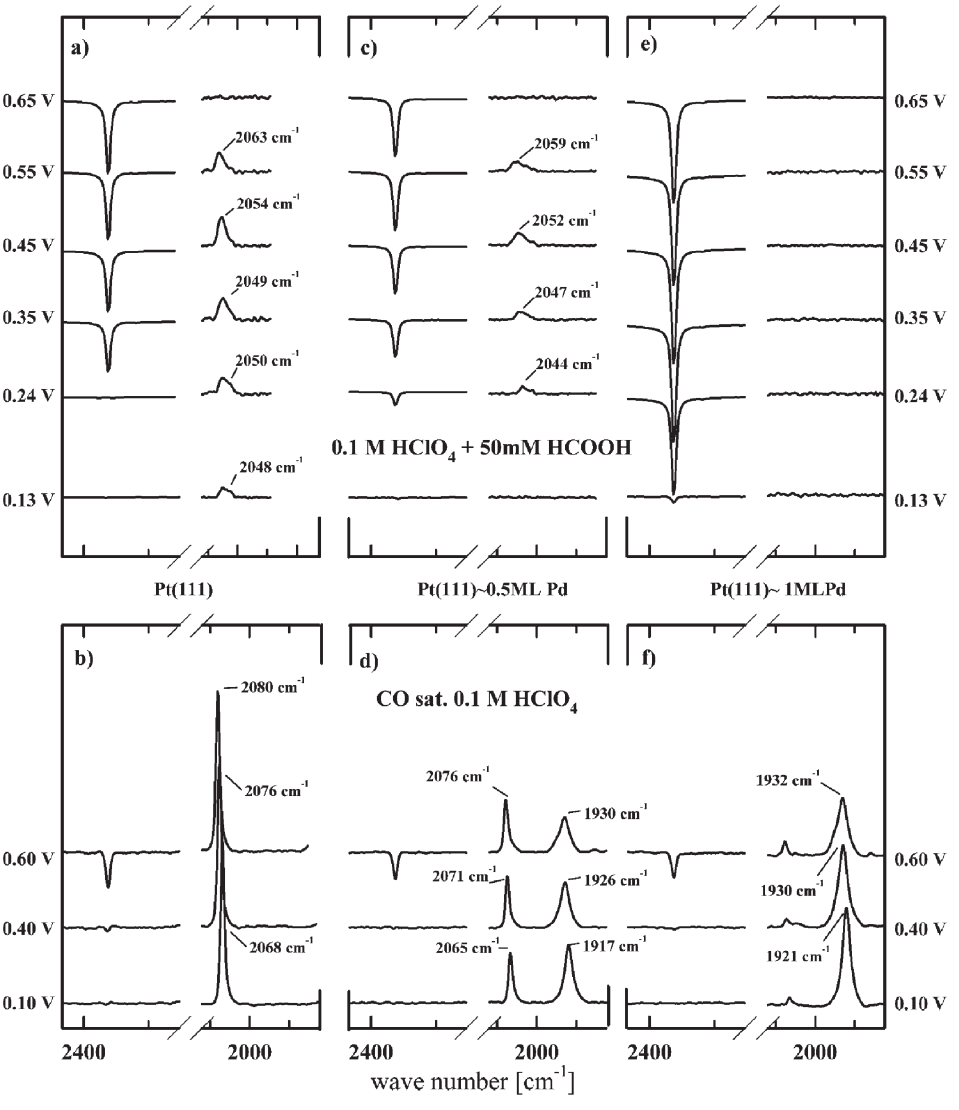

Fig. 4 (a, c, e): FTIR spectra recorded in 0.1 M $HClO_4$ containing 50 mM HCOOH; each potential is indicated in the figure. Reference spectra are recorded at 0.00 V for the spectral range of 2150–2450 cm^{-1} (CO_2 band) and at 1.0 V for the spectral range of 1850–2150 cm^{-1} (CO band). CO_2 bands are divided by a factor of 20. (b, d, f) Sets of spectra (divided by a factor of 2) for the same surfaces in CO saturated perchloric acid are shown for comparison. (a, b) Pt(111); (c, d) Pt(111)–$Pd_{\sim 0.5\ ML}$; (e, f) Pt(111)–$Pd_{\sim 1\ ML}$.

dehydration yields to consistently lower values in the frequency of the CO absorption band (*ca.* 35 cm^{-1} decrease) than the saturated CO layer formed by direct CO chemisorption.

Following the discussion by Weaver and co-workers,[8,9] these differences can readily be attributed to a lower surface CO coverage induced by the dehydration reaction of formic acid. Further inspection of Fig. 4a indicates that for $E < 0.35$ V the CO adsorption band can be observed without the formation of CO_2, implying that neither CO oxidation nor the dehydrogenation reaction takes place at low potentials. In contrast, for $0.3 < E > 0.45$ V a CO_2 band develops simultaneously with an increase in the amplitude of the CO stretching band. Notice, that in CO dosing experiments (Fig. 4b) CO_2 production is observed only above 0.4 V. Further inspection of Fig. 4a reveals that at potentials above 0.45 V the amplitude of the CO vibrational band decreases and that at $E > 0.6$ V adsorbed CO is no longer detected.

Corresponding FTIR spectra for Pt(111)–$Pd_{\sim 1\ ML}$ are shown in Fig. 4e. Interestingly, while a high rate of CO_2 production is observed even at low potentials ($E \approx 0.15$ V), *no* C–O stretching features are visible in the FTIR spectra at any potential. This finding, which is reproducible, strongly indicates that the reaction pathway for HCOOH oxidation on Pt(111) is completely different from that on the Pt(111)–$Pd_{\sim 1\ ML}$ surface. The binding site occupancy of CO and the corresponding CO_2 production on Pt(111)$Pd_{\sim 0.5\ ML}$ are also shown in Fig. 4. Inspection of the FTIR spectra in Fig. 4c illustrates two key points. First, while Pt–CO vibrational bands are observed *no* CO stretching bands are detected that correspond to the CO adsorption on Pd sites of the Pt(111)$Pd_{0.5\ ML}$ surface (see reference spectrum in Fig. 4d). A comparison between the corresponding CO spectra in Fig. 4a and 4c reveals similar band shapes for Pt–CO but the band center on the latter surface is red-shifted, between 6 to 2 cm^{-2}, depending on the electrode potential. This indicates that the CO islands formed from the dehydration of HCOOH are smaller on Pt(111)–$Pd_{\sim 0.5\ ML}$ than on bare Pt(111), consistent with a reduced number of Pt surface atoms. Secondly, CO_2 formation on Pt(111)–$Pd_{\sim 0.5\ ML}$ is observed as low as 0.24 V, *i.e.*, at the same potential where CO_2 formation is observed at the Pt(111)–$Pd_{\sim 1\ ML}$ surface. These two observations are consistent with the supposition in section 3.2.1 that Pt and Pd behave independently according to their own surface chemistry.

FTIR measurements of the $PtPd_{x at\%}(111)$ single crystal bulk alloys were performed in perchloric acid solution containing HCOOH as well as in a solution saturated with CO. Even though FTIR spectra were recorded on different samples, only the bulk alloy with 6 at% of Pd will here be introduced as an example to demonstrate all important features of HCOOH/CO surface electrochemistry on Pt–Pd single crystal bulk alloys. The potential-dependent series of FTIR spectra of the $PtPd_{6at\%}(111)$ bulk alloy in $HClO_4$ solution containing 50 mM HCOOH is shown in Fig. 5a. In the potential region between 0.1–0.7 V, a single C–O stretching band can be distinguished at 2023–2055 cm^{-1}. The FTIR spectra for CO dosing are shown in Fig. 5b. For the $PtPd_{6at\%}(111)$ bulk alloy surface, only one peak due to linear bonded CO (at 2058–2071 cm^{-1}), is observed, in agreement with previous proposition that Pt and Pd are atomically mixed at the surface. Furthermore, in comparison with Pt(111) (Fig. 4a), substantial (up to 10 cm^{-1}) CO frequency red-shifts are seen for CO on $PtPd_{6at\%}(111)$. Comparison of Fig. 5a and 5b reveals that formic acid dehydration yields consistently lower vibrational CO bands (*ca.* 35 cm^{-1}) and higher Stark-tuning slopes, *i.e.* shift of the absorption frequency with applied potential (*ca.* 10 cm^{-1} V^{-1}, not shown), than the saturated CO layer formed by direct CO adsorption in accordance with the fact that the CO_{ad} adlayer produced from the HCOOH dehydration reaction has a lower overall density than the adlayer produced by CO

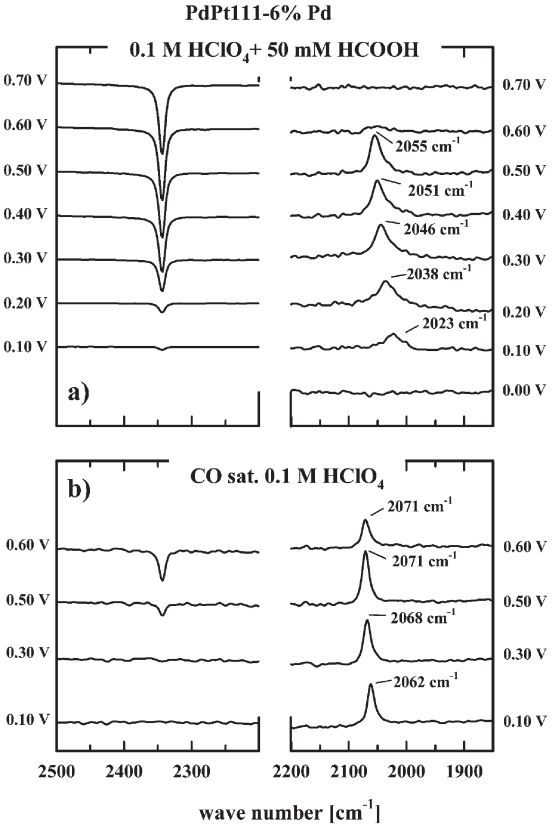

Fig. 5 FTIR spectra of the $PtPd_{6at\%}(111)$ bulk alloy recorded in (a) 0.1 M $HClO_4$ containing 50 mM HCOOH and (b) CO sat. 0.1 M $HClO_4$; each potential is indicated in the figure. Reference spectra are recorded at 0.00 V for the spectral range of 2150–2450 cm^{-1} (CO_2 band) and at 1.0 V for the spectral range of 1850–2150 cm^{-1} (CO band). The intensities of the spectra at the left hand side (CO_2 bands) of part (a) (HCOOH containing solution) are divided by 10 compared to the right hand side of part (a).

dosing experiments. Finally, a close inspection of Fig. 5a shows that a small but continuous production of CO_2 takes place at 0.2 V, in harmony with the onset of HCOOH dehydrogenation observed in Fig. 4e.

3.2.3. Temperature effects. Given that the HCOOH oxidation on Pd atoms proceeds without the formation of CO_{ad}, we conclude that the strong deactivation observed in Fig. 2a and 2b is not due to the formation of a "poisoning" intermediate. As we pointed out in section 3.2.1 the deactivation may be caused by the blocking of active sites due the adsorption of spectator species such as OH_{ad} and/or $ClO_{4,\ ad}$ and Cl_{ad}. In order to get further insight into the effects of OH_{ad}, we studied the effect of temperature on the kinetics of formic acid oxidation on Pt(111)–$Pd_{0.2ML}$. As already discussed in section 3.2.1, on this surface the *I vs. E* relationship can be divided into two potential regions. The low potential region ($0.05 < E < 0.4$ V) corresponds to the oxidation of HCOOH on Pd islands and at higher potentials ($0.4 < E > 0.9$ V) the polarization curve is similar to the one observed on the bare Pt(111) surface. From Fig. 6 it can be seen that the temperature and scan direction have a different effect on Pt and Pd surfaces atoms, respectively. Namely, while there is little difference in the catalytic activity between the positive and negative sweep directions in the "Pt-potential region", the activity in the "Pd-potential region" is much higher during the positive than the negative potential sweep. This behavior is consistent with the fact that Pd atoms are more oxophilic than Pt atoms and thus at higher temperatures a more stable oxide can be formed on the former surface. As a consequence, the number of active sites (created by the reduction of Pd-oxide) available for the adsorption of

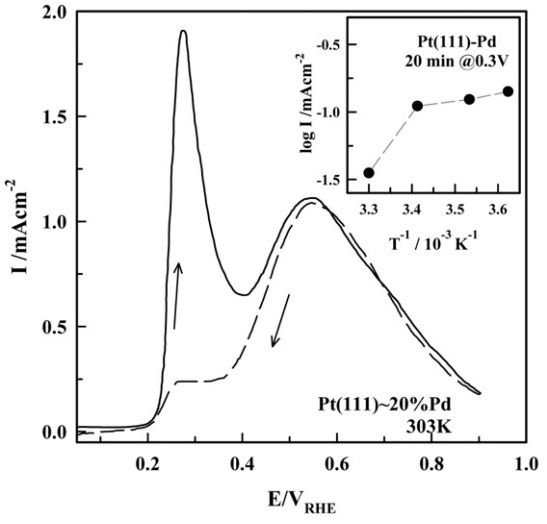

Fig. 6 Polarization curve recorded on Pt(111)–$Pd_{\sim 0.2\ ML}$ at 303 K in 0.1 M $HClO_4$ containing 50 mM HCOOH. Sweep rate 10 mV s^{-1}; positive going (——) and negative going (– – –) scan indicated by arrows; inset: Arrhenius plot of the steady state-current density *vs.* inverse temperature recorded on a Pt(111)–$Pd_{\sim 1\ ML}$ electrode 20 min after a potential step from 0.05 V.

the HCOOH molecule is significantly reduced in the "Pd-potential region" during the negative potential sweep. In the inset of Fig. 6, the deactivation by the temperature-induced oxide formation on Pd is even more obvious. The steady-state (20 min) current densities at the Pt(111)–$Pd_{\sim 1\ ML}$ interface at a potential of 0.3 V after a potential step from 0.05 V are summarized in an Arrhenius plot. It can be clearly seen, that increasing the temperature of the supporting electrolyte in the temperature range between 276 and 303 K gives rise to a *deactivation* of the surface in contrast to an *activation* which was previously observed for the same procedure but on bare Pt(111).[27]

4. Discussion

A consensus now appears to exist that in the electrochemical environment, the oxidation of formic acid on Pt group metals proceeds *via* the dual path mechanism originally proposed by Capon and Parsons.[7] Our version of this mechanism is the following reaction scheme:[3]

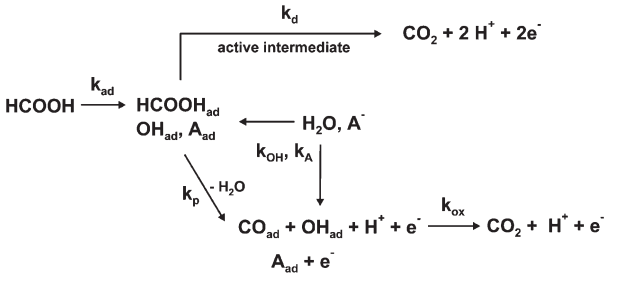

In this reaction scheme the first step, the adsorption of HCOOH on the surface (k_{ad}), is in competition with the adsorption of spectator species, *viz.* H_{upd} (k_H), anions (k_A) and OH_{ad} (k_{OH}).[27] It was found that HCOOH can easily be displaced from the surface by these spectator species[1,3] and hence in an electrochemical environment the adsorption of HCOOH molecules may occur only on an ensemble of bare (water modified) metal sites. In the simplest terms, the notation "spectator species" defines a species that impedes the electro-oxidation of formic acid by blocking the active sites required for the adsorption of HCOOH molecules. In the present case, these spectator species can be formed from H^+ (H_{upd}), ClO_4^- ($ClO_{4,\ ad}$), Cl^-(Cl_{ad}) and H_2O (OH_{ad}). It is important to note, that H_{upd}, $ClO_{4,\ ad}$ and Cl_{ad} behave as "poisoning" species in the entire potential region, while in contrast OH_{ad} may have two modes of action on the electro-oxidation of formic acid: at higher overpotentials OH_{ad} is a poison (blocking species), whereas at low overpotentials OH_{ad} is a reactive intermediate, which can react with adsorbed CO formed from the dehydration reaction of HCOOH.[3] According to the reaction scheme above, adsorbed HCOOH can be either "directly" oxidized to CO_2, *via* a dehydrogenation reaction step (k_d), or it can form poisoning reaction intermediates *via* a (non-faradaic) dehydration reaction step (k_p). The nature of the "poisoning species" (*i.e.*, strongly bonded adsorbed intermediates) which are formed during the electrochemical oxidation of formic acid on metal surfaces has been the subject of controversy for a long time.[1] The notation of "poisoning" intermediate refers to an adsorbed species, formed directly from the reactant, which impedes the reaction *via* other intermediates by hindering their formation and/or their oxidative conversion to CO_2. It has been suggested that these species are either CO[29–31] or intermediates containing both hydrogen and oxygen bonds, *viz.* COH and HCO.[32–35] On the basis of recent FTIR studies,[8,10] and in agreement with our results shown in Fig. 4a, the major "poisoning" species involved in formic acid oxidation on a Pt electrode was clearly identified as carbon monoxide. As mentioned above for OH_{ad}, there is also the possibility that in a certain potential region adsorbed CO may act as a reaction intermediate rather than as a catalytic poison. Therefore, CO may also provide a reaction channel to CO_2 production under certain conditions where there is a surface reaction with OH_{ad} formed from the dissociation of water.[3] In what follows, using the proposed reaction scheme and the results described in section 3 we will try to get some insight into the mechanism/reaction pathway of the electro-oxidation of formic acid first on Pt(111) and then on Pt(111)–Pd bimetallic surfaces.

4.1 Pt(111) system

Very recently, Osawa and co-workers[36] used surface-enhanced IR absorption spectroscopy (SEIRAS) on Pt nanoparticles in acid solution containing HCOOH, and reported in addition to the commonly observed linear and bridging CO bands, a band at *ca.* 1320 cm^{-1}. This band was reported to shift with potential from 1320 cm^{-1} (0.6 V) to 1328 cm^{-1} (1.25 V), indicating that the band comes from an adsorbed species. Following gas phase assignments,[37] this band was assigned to the symmetric OCO stretching mode of formate (HCOO) adsorbed on the Pt surface with a bridging configuration. In our IR experiments, no band corresponding to formate was observed, although great effort and great care were given for its observation. Considering that in SEIRAS the absorption from molecules adsorbed on metal nanoparticles is significantly enhanced (factor of *ca.* 100) relative to IRAS intensities, it is perhaps not surprising that only CO adsorption bands are observed in the spectra depicted in Fig. 4.

One approach to ascertain whether the oxidation of HCOOH on Pt proceeds through a dehydrogenation or a dehydration reaction is to compare IRAS spectra of a CO adlayer formed on Pt *via* formic acid dissociation with IRAS spectra of a CO adlayer formed by direct chemisorption in CO saturated (1 atm) solution. While CO_2 formation and C–O stretching (ν_{CO}) bands are observed for both systems (Fig. 4a and 4b), significant differences are evident. First, the ν_{CO} frequencies obtained from the HCOOH dehydration reaction are *ca.* 20 cm^{-1} lower compared to those obtained at a given electrode potential for the adsorption from CO dissolved in the solution. This observation suggests that the CO coverage produced from HCOOH is well below saturation coverage.[9,38]

A second obvious difference concerns the onset potential for CO_2 formation. While the CO_2 band produced from HCOOH appears as low as 0.35 V, CO_2 formation in CO saturated solution is observed only above 0.4 V. The fact that in the HCOOH containing solution below 0.35 V CO_{ad} is produced without the formation of CO_2 implies that HCOOH oxidation proceeds at low overpotentials exclusively through the dehydration reaction pathway,

$$HCOOH \xrightarrow[-H_2O]{} CO_{ad} + H_2O \quad (1)$$

Given that even in SEIRAS experiments neither formate nor carboxyl (–COOH) have been found below 0.5 V, it is difficult to resolve what reactive intermediate might be formed as a precursor for the formation of CO below 0.35 V. At higher overpotentials, while a substantial CO_2 band is observed as low as 0.35 V, a rather small increase in the ν_{CO} intensity is obtained between 0.35–0.45 V. These results strongly suggest that above 0.35 V the electro-oxidation of HCOOH proceeds rather through the dehydrogenation than the dehydration reaction pathway, *i.e.* in agreement with Osawa and co-workers,[36]

$$HCOOH \xrightarrow[-H]{} HCOO_{ad} \xrightarrow[-H]{} CO_2 + 2H^+ + 2e^- \quad (2)$$

Fig. 4a shows that by applying more positive potentials than 0.45 V, ν_{CO} intensities decrease and at 0.6 V no visible ν_{CO} is observed in the spectra. This indicates that above $E > 0.45$ V, CO_2 can be produced simultaneously from the dehydrogenation reaction (eqn. (2)) and from the oxidative removal of CO_{ad} (which is formed below 0.45 V),

$$CO_{ad} + OH_{ad} = CO_2 + H^+ + e^- \quad (3)$$

In line with the CO oxidation on Pt(111) discussed in ref. 39 we attribute CO_{ad} oxidation below 0.6 V to the adsorption of OH_{ad} at defect sites in the Pt(111) surface. A comparison of the results in Fig. 1 and the polarization curves for the HCOOH oxidation in ref. 27 reveals that the maximum rate of HCOOH oxidation on Pt(111) is obtained at 0.6 V, *i.e.*, at the potential where the oxidative removal of CO_{ad} is optimized by a minimum surface coverage of OH_{ad}. At higher potentials, when excess of OH_{ad} is not consumed in the Langmuir–Hinshelwood (L–H) surface reaction, OH_{ad} begins to behave as a poisoning species (see above), similar as for methanol electro-oxidation on Pt in acid and alkaline solutions.[1]

4.2 Pt(111)–Pd_{xML} systems

A markedly different behavior, however, was obtained for formic acid electro-oxidation on Pt modified with 1 ML of Pd. For example, the characteristic stretching bands for a CO adlayer formed on the Pt(111)–$Pd_{\sim 1\ ML}$ surface in CO saturated solution (Fig. 4f) cannot be observed in perchloric acid solution containing HCOOH (Fig. 4e). Our FTIR results are consistent with previous conclusions, inferred from classical electrochemical measurements, that the formation of CO_{ad} on both Pt single crystals modified with Pd films[25] as well as on a polycrystalline Pt/Pd electrode[26] does not occur or occurs at a very slow rate. Our results in Fig. 4 unambiguously demonstrate that the reaction pathway on Pd is indeed completely different from that on Pt, *i.e.*, the oxidation of HCOOH on the Pt(111)$Pd_{1\ ML}$ surface proceeds *exclusively* through the dehydrogenation reaction pathway described by the eqn. (2). As for Pt(111), no band of a formate intermediate was observed at any potential. Interestingly, in UHV experiments Davis and Barteau identified formate as the intermediate in the HREEL spectra[40] for formic acid decomposition on Pd(111).[37] It is possible that formate is also a reaction intermediate in the electrochemical environment. SEIRAS experiments with nanocrystalline Pd may help to clarify the nature of the reaction intermediates formed at the Pd surface.

At this point it is also important to emphasize that although at low overpotentials Pd surface atoms are very active for formic acid oxidation it is still puzzling why a deactivation occurs in a very narrow potential region as well as why the electrocatalytic activity is inhibited at low sweep rates (1 mV s^{-1}). As pointed out in the previous section, for the electrocatalysis of HCOOH oxidation the formation of a self-poisoning intermediate (CO_{ad}) is often proposed to have a major role in the observed deactivation.[1,3] Our FTIR results presented in Fig. 4e, however, reveal that CO is not formed during HCOOH oxidation on Pd and hence some other species have to be responsible for the observed deactivation. As mentioned in the previous section, other authors came to the same conclusion based either on cyclic voltammetry[25] or on a combination of cyclic voltammetry and chronoamperometry[26] measurements. In the latter study the authors suggested that on Pt and Pt/Pd the current decay at potentials higher than 0.45 V results from the interference of interfacial CO_2 and/or the adsorption of formic acid (formate anions). In contrast, and in line with our discussion for the effects of oxide formation and specific anion adsorption on the methanol oxidation on Pt(*hkl*),[41] we suggest here that the strong adsorption of OH and/or $ClO_{4,\ ad}$ and Cl anions may impede the reaction on Pd even at very low potentials. This proposition is strongly supported by the influence of the electrolyte temperature on the kinetic rate of HCOOH oxidation. The anomalous decrease of the oxidation currents with increasing temperature, illustrated in Fig. 6, is attributed to the temperature dependent increase of OH adsorption on Pd atoms, the (excess) OH_{ad} in this potential region being a blocking species. Our explanation, therefore, for the relatively rapid deactivation at low overpotentials in Fig. 2a and 2b is the adsorption of spectator OH_{ad} species which block the active sites required for the adsorption of HCOOH.

Having established the catalytic behavior of Pt(111) and Pt(111) covered with a pseudomorphic Pd monolayer, we continue our discussion by focusing on the catalytic properties of Pt(111) modified by a Pd submonolayer. We recall that the FTIR characterization of Pt(111) modified with $0 < \Theta_{Pd} < 1$ ML in ref. 21 and 22 and in Fig. 4d was used to establish whether Pd forms 2D islands or Pd atoms are dispersed on the surface much more randomly, as seen for the deposition of Bi on transition metals.[42] The appearance of two different C–O stretching bands which are characteristic for unmodified Pt and Pt covered with one Pd ML in the FTIR spectra of the Pt(111)–$Pd_{\sim 0.5\ ML}$ surface implies that Pd atoms cluster into islands (see model in Fig. 7). From these results one would expect a gradual change in the catalytic properties from those characteristic for bare Pt(111) to those which are characteristic for the Pt(111)–$Pd_{\sim 1\ ML}$ electrode. In Figs. 2 and 4 it is shown that this is in fact the case for the electro-oxidation of HCOOH and the adsorption of CO. For example, Fig. 2b shows that on the Pt(111)–$Pd_{\sim 0.2\ ML}$ surface two potential regions are clearly visible in the polarization curves; at low potentials the Pd-like activity and at higher potentials the Pt-like activity. This observation is in agreement with our supposition that Pt and Pd on Pt(111) modified with a Pd submonolayer behave according to their singular surface chemistry. Further evidence for this supposition is obtained from the FTIR spectra depicted in Fig. 4. In particular, for the Pt(111)–$Pd_{\sim 0.5\ ML}$ surface exposed to formic acid (Fig. 4c), both a characteristic Pt–CO band frequency (the Pt fingerprint) and CO_2 production at low potentials (the Pd fingerprint) are clearly resolved in spectra. Notice that CO_2 production from a CO adlayer formed in CO saturated solution is detected only above 0.4 V, *i.e.*, well above the potential for CO_2 production in Fig. 4c. One could argue that the observed difference arises due to lower CO coverage formed from formic acid and the more facile oxidation of CO adsorbed on Pt with OH adsorbed on Pd sites, *i.e.*, the bifunctional effect. However, from UHV and electrochemical measurements

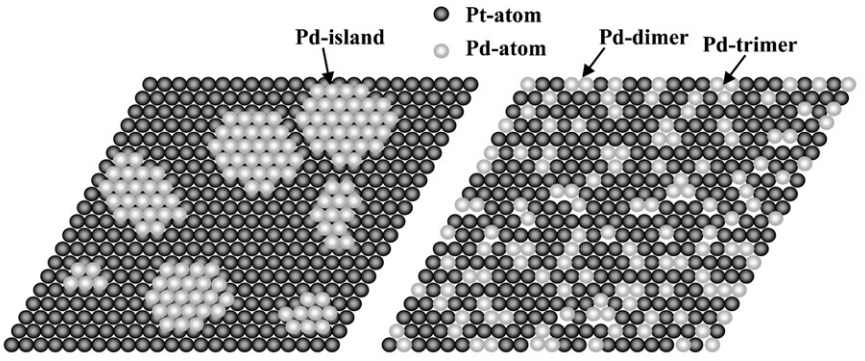

Fig. 7 Ball model of a Pd film on the Pt(111) surface and a $PtPd_{x at\%}(111)$ bulk alloy with the same Pd surface coverage of about 0.28.

it is well known that with increasing coverage the CO adsorption energy decreases due to repulsive CO–CO interactions, and hence CO is more easily oxidized at higher, not lower, coverage.[3] Furthermore, despite the fact that the adsorption of OH is enhanced on the Pd sites, recently we observed that the (continuous) oxidation rate of CO (dissolved in solution) is considerably lower on Pd-modified Pt(111) than on bare Pt(111)[22] and the peak potential in CO stripping curves is shifted to higher values for Pd-modified Pt surfaces. The same effect is displayed in the data presented here by the fact that the intensities of the CO_2 bands in the spectra of Fig. 4b, d, f) decrease with the Pd coverage on the surface. It appears, that at the Pt(111)–$Pd_{x ML}$ interface OH_{ad} adsorbed on the Pd atoms plays only a minor role in the oxidative removal of CO_{ad} from the Pt sites and, thus, the bifunctional mechanism is not operative at the Pt(111)–$Pd_{x ML}$ surfaces as it is for example for PtRu bimetallic surfaces.[43] One reason for this could be a decreased mobility of CO_{ad} on a Pt(111)–$Pd_{x ML}$ surface. However, so far we have no indication for this, and as an explanation for the results, we suggested that the Pd–OH interaction is too strong to effectively oxidize adsorbed CO.[22]

4.3 $PtPd_{x at\%}(111)$ systems

As mentioned above, in contrast to the Pt(111)–$Pd_{x ML}$ systems, the oxidation of HCOOH (Fig. 2c–2d and Fig. 5a) and CO (Fig. 5b) on the $PtPd_{x at\%}(111)$ bulk alloys indicates synergetic properties, which cannot be rationalized by a mere linear superposition of the properties of the pure metals. This point becomes clear from the results depicted in Fig. 2c and 2d which show that the polarization curves for the formic acid oxidation cannot be unambiguously divided into Pd-like and/or Pt-like potential regions, although the onset of oxidation is Pd-like. Another example of a rather strong synergy between Pd and Pt atoms is seen from the properties of the CO adlayer which is formed on the $PtPd_{6at\%}(111)$ surface by direct chemisorption from a CO saturated solution. Clearly, only a band similar to linearly bonded Pt–CO appears in the FTIR spectra, as evidenced by the C–O stretch features at 2062–2071 cm^{-1}. A close inspection of the spectral data reveals that CO bound to the $PtPd_{6at\%}(111)$ alloy exhibits frequency values that are red-shifted from atop CO_{ad} on Pt(111) and significantly blue-shifted from the bridge-bonded CO_{ad} on Pd(111). Such a frequency/site-occupancy change has been noted previously for the adsorption of CO on a PtRu bulk alloy and has been attributed to the vibrational coupling between CO adsorbed on a more or less random arrangement of Pt and Ru surface atoms.[44] If we extend this phenomenon to Fig. 5d, a shift of the CO frequency on the $PtPd_{6at\%}(111)$, from those characteristic for bare Pt(111) is indicative of a dipole–dipole coupling between CO adsorbed on both Pt and Pd sites, consisting of a mixture of single Pd atoms, Pd dimers, and Pd trimers (Pd ensembles), which are formed *in* a "sea" of Pt atoms (see model in Fig. 7). This would be in line with the prediction based on the bulk phase diagram of the Pd–Pt system, whereby both metals form a continuous series of solid solutions[45] and the LEIS data, which indicate that the surface is enriched with palladium after both thermal equilibrium in UHV and cooling in a hydrogen atmosphere.[20] A striking feature of the results presented here is the marked difference in the dynamic dipole–dipole coupling of CO_{ad} at the $PtPd_{x at\%}(111)$ and the Pt(111)–$Pd_{x ML}$ surfaces. In particular, unlike the $PtPd_{6at\%}$-(111)–CO system, on the Pt(111)–$Pd_{x ML}$ surface there is no vibrational coupling discernible between CO patches formed on the Pt substrate and on two-dimensional Pd islands. This may be understood by the models presented in Fig. 7, which display the expected surface arrangement for the two differently prepared surfaces: (i) the Pd film where Pd is expected to cluster into large islands *on* the Pt substrate and hence the expected behavior of a CO adlayer is a linear superposition of the behavior for the Pt–CO and Pd–CO interaction; and (ii) an atomically dispersed structure, composed of Pd nanoclusters incorporated *into* the surface. Clearly, the absence of the formation of large two dimensional Pd islands in the $PtPd_{6at\%}(111)$ surface results in a coupling between Pt–CO and Pd–CO and hence in a deviation of the CO frequency from those frequencies which are characteristic for the pure metals.

In discussing the reaction mechanism of HCOOH oxidation on the $PtPd_{x at\%}(111)$ surfaces, we should re-emphasize the observations stated in section 3.3, *viz.* that a CO adlayer formed *via* the dehydration reaction, as evidenced by the potential dependent C–O stretch features and CO_2 formation, is stable from 0.1–0.5 V and that the onset of CO_2 formation starts at potentials as low as 0.2 V. In general, CO_2 may be produced either by the oxidative removal of CO in the L–H type reaction or through the dehydrogenation reaction step. As demonstrated by the CO dosing experiments shown in Fig. 5b, CO oxidation (CO_2 production) occurs only at potentials higher than 0.3 V. Therefore, it is reasonable to conclude that at the $PtPd(111)_{6at\%}$ surface the CO_2 observed at 0.2 V in the solution containing HCOOH is rather produced from the dehydrogenation reaction step than from the oxidative removal of CO_{ad}. In contrast to the behavior observed for a CO adlayer produced in a CO saturated solution, the oxidation of HCOOH on the $PtPd_{x at\%}(111)$ bulk alloys also displays features indicating that the reaction (partially) proceeds according to the singular Pt and Pd surface chemistry, *i.e.*, HCOOH oxidation may occur (to some extent) independently on Pd ensembles and on the Pt substrate. Indications for this conclusion can be found in the FTIR spectra by the fact that the onset of CO_2 production can be clearly observed at 0.2 V and concomitantly ν_{CO} is produced already at 0.1 V. These two features can be assigned to Pd-like and Pt-like behavior respectively. Furthermore, the polarization curves in Fig. 2c, d,) show, that for $PtPd_{25at\%}(111)$ the onset of HCOOH oxidation is concurrent with the onset on the Pd films. The origin of these differences in behavior between CO and HCOOH can be

traced back in part to the interaction of dissolved HCOOH and CO with the $PtPd_{6at\%}(111)$ surface. For the pure metal–CO systems, CO adsorption energies on Pt(111) and Pd(111) surfaces are within ±10% the same, *viz.* about 140 KJ mol^{-1} for a high surface coverage,[46] indicating very little difference in the CO chemisorption properties of these two metals. That is, CO is adsorbed equally easily on Pt and on Pd atoms. This behavior, together with the fact that Pd atoms in the ensembles are *always* surrounded by Pt atoms (see the model in Fig. 7b) can induce a close coupling between CO that is adsorbed on Pt and Pd sites. For the metal–HCOOH systems, however, at low potentials where Pd is very active for the electro-oxidation of HCOOH, the interaction of formic acid with Pt is quite different from that with Pd. Namely, assuming the direct pathway on Pd *via* the formate intermediate, Pd has a strong tendency to break the O–H bond in the HCOOH molecule, whereas Pt at low potentials has a stronger tendency to break a C–O bond (or first the C–H and then the C–O bond). Various details of HCOOH adsorption on Pt and Pd in an electrochemical environment are, however, still unresolved and some future theoretical aspects of the relationship between the electronic structure and adsorptive chemistry could be useful in order to understand the differences in catalytic activity of Pt and Pd atoms in electrocatalysis of HCOOH.

5. Conclusion

It was shown that Pd atoms either *on* the surface or *in* the surface have an unique catalytic activity for HCOOH oxidation, with Pd atoms being about three (bulk alloys) to five times (Pd films) more active than Pt atoms at 0.4 V. This difference in activity can be attributed to the fact that the reaction pathway for formic acid electro-oxiation is different on both metals. At low potentials on Pt atoms formic acid electro-oxiation results always in adsorbed CO, which is produced from the HCOOH dehydration pathway. Thus on Pt the reaction is self-poisoning in the low potential region, where CO_{ad} cannot be oxidized further. In contrast, for Pt–Pd bimetallic surfaces in HCOOH containing electrolyte, *no* vibrational features for Pd–CO can be observed, although high CO_2 production rates are observed at potentials as low as ≈0.15 V. These results indicate, that the interaction of the formic acid molecule with Pt and Pd atoms is completely different. While Pd has in the entire potential region a propensity to break only the O–H bonds of the HCOOH molecule, Pt seems to have a propensity to break both the C–O and/or C–H bond (at low potentials) as well as the O–H bond (at higher potential). Consequently, HCOOH oxidation on Pd atoms proceeds *exclusively* through the dehydrogenation reaction step, while on Pt at low potentials the dehydration reaction pathway is predominant.

Furthermore, the results for the electro-oxidation of HCOOH on $Pt(111)–Pd_{x ML}$ surfaces reveal, that Pt and Pd surface atoms behave according to their singular surface chemistry, whereas for $PtPd_{xat\%}(111)$ surfaces indications of both a small synergetic effect of Pt and Pd as well as an independent behavior of the two metals can be found. This is in contrast to the adsorption of the CO molecule. FTIR results show that CO adsorption on Pt–Pd bimetallic surfaces is strongly dependent on the position/distribution of the Pd surface atoms. If Pd atoms are dispersed *in* the Pt surface (the $PtPd_{xat\%}(111)$ systems) adsorbed CO, which is adsorbed on both Pd and Pt atoms, exhibits strong dipole coupling, whereas on $Pt(111)–Pd_{\sim x ML}$ surfaces, there is no vibrational coupling between Pt–CO and Pd–CO discernible.

Acknowledgements

This work was supported by the Director, Office of Science, Office of Basic Energy Sciences, Division of Materials Sciences, U.S. Department of Energy under Contract No. DE-AC03-76SF00098. M. A. gratefully acknowledges a Feodor Lynen Fellowship from the Alexander von Humboldt Foundation of Germany. The authors are indebted to G. A. Attard (University Cardiff, UK) for providing the $PtPd_{xat\%}(111)$ alloy beads.

References

1 R. Parsons and T. VanderNoot, *J. Electroanal. Chem.*, 1988, **257**, 9.
2 A. Hamnet, *Interfacial Electrochemistry*, Marcel Dekker, Inc., New York, 1999.
3 N. M. Markovic and J. Ross, *Surf. Sci. Rep.*, 2002, **45**, 117–229.
4 V. R. Stamenkovic, M. Arenz, C. A. Lucas, M. E. Gallagher, P. N. Ross and N. M. Markovic, *J. Am. Chem. Soc.*, 2003, **125**, 2736–2745.
5 Y. X. Chen, A. Miki, S. Ye, H. Sakai and M. Osawa, *J. Am. Chem. Soc.*, 2003, **125**, 3680–3681.
6 S. Park, A. Wieckowski and M. J. Weaver, *J. Am. Chem. Soc.*, 2003, **125**, 2282–2290.
7 A. Capon and R. Parsons, *J. Electroanal. Chem.*, 1973, **45**, 205.
8 S. C. Chang, Y. Ho and M. J. Weaver, *Surf. Sci.*, 1992, **265**, 81–94.
9 S. C. Chang, L.-W. H. Leung and M. J. Weaver, *J. Phys. Chem.*, 1990, **94**, 6013–6021.
10 T. Iwasita, X. H. Xia, E. Herrero and H. D. Liess, *Langmuir*, 1996, **12**, 4260–4265.
11 M. D. Macia, E. Herrero and J. M. Feliu, *Electrochim. Acta*, 2002, **47**, 3653–3661.
12 M. D. Macia, E. Herrero, J. M. Feliu and A. Aldaz, *J. Electroanal. Chem.*, 2001, **500**, 498–509.
13 N. M. Markovic, H. A. Gasteiger, P. N. Ross, X. D. Jiang, I. Villegas and M. J. Weaver, *Electrochim. Acta*, 1995, **40**, 91–98.
14 H. A. Gasteiger, N. Markovic, P. N. Ross and E. J. Cairns, *Electrochim. Acta*, 1994, **39**, 1825–1832.
15 E. Herrero, J. M. Feliu and A. Aldaz, *J. Electroanal. Chem.*, 1994, **368**, 101–108.
16 N. Kizhakevariam and M. J. Weaver, *Surf. Sci.*, 1994, **310**, 183–197.
17 E. Leiva, T. Iwasita, E. Herrero and J. M. Feliu, *Langmuir*, 1997, **13**, 6287–6293.
18 X. H. Xia and T. Iwasita, *J. Electrochem. Soc.*, 1993, **140**, 2559–2565.
19 P. N. Ross, *Electrocatalysis*, Wiley-VCH, 1998.
20 T. J. Schmidt, N. M. Markovic, V. Stamenkovic, P. N. Ross, G. A. Attard and D. J. Watson, *Langmuir*, 2002, **18**, 6969–6975.
21 M. Arenz, V. Stamenkovic, T. J. Schmidt, K. Wandelt, P. N. Ross and N. M. Markovic, *Surf. Sci.*, 2002, **506**, 287–296.
22 M. Arenz, V. Stamenkovic, T. J. Schmidt, K. Wandelt, P. N. Ross and N. M. Markovic, *Surf. Sci.*, 2003, **523**, 199–209.
23 K. Ataka, T. Yotsuyanagi and M. Osawa, *J. Phys. Chem.*, 1996, **100**, 10 664–10 672.
24 M. J. Llorca, J. M. Feliu, A. Aldaz and J. Clavilier, *J. Electroanal. Chem.*, 1994, **376**, 151–160.
25 M. Baldauf and D. M. Kolb, *J. Phys. Chem.*, 1996, **100**, 11 375–11 381.
26 G. Q. Lu, A. Crown and A. Wieckowski, *J. Phys. Chem. B*, 1999, **103**, 9700–9711.
27 T. J. Schmidt, R. J. Behm, B. N. Grgur, N. M. Markovic and P. N. Ross, *Langmuir*, 2000, **16**, 8159–8166.
28 A. Gil, A. Clotet, J. M. Ricart, F. Illas, B. Alvarez, A. Rodes and J. M. Feliu, *J. Phys. Chem. B*, 2001, **105**, 7263–7271.
29 A. Bewick, *J. Electroanal. Chem.*, 1983, **150**, 481–493.
30 K. Kunimatsu, *J. Electroanal. Chem.*, 1986, **213**, 149–157.
31 F. Hahn, B. Beden, F. Kadirgan and C. Lamy, *J. Electroanal. Chem.*, 1987, **216**, 169–180.
32 S. Juanto, B. Beden, F. Hahn, J.-M. Leger and C. Lamy, *J. Electroanal. Chem.*, 1987, **237**, 119–129.
33 J. Willsau and J. Heitbaum, *J. Electroanal. Chem.*, 1985, **185**, 181–183.
34 W. Vielstich, P. Christensen, S. A. Weeks and A. Hamnett, *J. Electroanal. Chem.*, 1988, **242**, 327–333.
35 S. Wilhelm, T. Iwasita and W. Vielstich, *J. Electroanal. Chem.*, 1987, **238**, 383–391.
36 A. Miki, S. Ye and M. Osawa, *Chem. Commun.*, 2002, 1500–1501.
37 M. R. Columbia and P. A. Thiel, *J. Electroanal. Chem.*, 1994, **369**, 1–14.
38 S. C. Chang and M. J. Weaver, *Surf. Sci.*, 1990, **238**, 142–162.

39 N. P. Lebedeva, M. T. M. Koper, E. Herrero, J. M. Feliu and R. A. van Santen, *J. Electroanal. Chem.*, 2000, **487**, 37–44.
40 J. L. Davis and M. A. Barteau, *Surf. Sci.*, 1991, **256**, 50–66.
41 N. Markovic and P. N. Ross, *J. Electroanal. Chem.*, 1992, **330**, 499–520.
42 M. T. Paffett, C. T. Campbell and T. N. Taylor, *J. Chem. Phys.*, 1986, **85**, 6176–6185.
43 H. A. Gasteiger, N. Markovic, P. N. Ross and E. J. Cairns, *J. Phys. Chem.*, 1994, **98**, 617–625.
44 R. Ianniello, V. M. Schmidt, U. Stimming, J. Stumper and A. Wallau, *Electrochim. Acta*, 1994, **39**, 1863–1869.
45 T. B. Massalski, *Metall. Trans. A*, 1989, **20A**, 1295–1323.
46 T. Engel and G. Ertl, *Adv. Catal.*, 1979, **28**.